

# Density dependent speed-up of particle transport in channels

Karolis Misiunas\* and Ulrich F. Keyser†  
Cavendish Laboratory, University of Cambridge, UK  
(Dated: May 6, 2022)

Collective transport through channels has surprising properties due to one-dimensional confinement: particles in a single-file exhibit sub-diffusive behaviour, while liquid confinement causes distance-independent correlations between the particles. Interactions in channels are well-studied for passive Brownian motion but driven transport remains largely unexplored. Here, we demonstrate a speed-up effect for actively driven particle transport through microfluidic channels. We prove that particle velocity increases with particle density in the channel due to hydrodynamic interactions. The magnitude depends on the driving force, where we measure and compare systems driven by electrophoretic and gravitational forces. We employ numerical models to demonstrate that the observed speed-up of transport originates from a hydrodynamic piston-like effect. Our discovery is fundamentally important for understanding protein channels, transport through porous materials, and for designing novel molecular sensors.

## Introduction

The diffusive and driven motion of solute particles confined in channel-like geometries depends on the interplay of different interactions; often giving rise to unexpected and even counter-intuitive behaviour. One landmark study showed that local interactions can produce sub-diffusive motion in single-file systems [1]. In even tighter confinement, molecules can move with unexpected velocities through channels lined with carbon atoms [2, 3]. Another counter-intuitive phenomenon is the coupling of particles via long-range interactions that are independent of the particle spacing [4]. Common to all these effects is the importance of confinement shape, the relevant forces, and boundary conditions. Their combination leads to novel physical effects, that are often most obvious in single-file systems.

Understanding such particle transport is important for fundamental physics as well as in applied sciences. Life depends on biomolecular transport through narrow protein channels [5], where the physical models of transport are now employed in computer aided drug design [6]. Narrow channels are also essential in novel DNA sequencing approaches [7] as well as for identifying biomolecules [8]. For transport through porous media consisting of a network of interconnected narrow channels, a speed-up of transport is required for increased efficiency of oil extraction, molecular separation [9] and for next-generation batteries [10]. All these examples rely on particles, ions or molecules driven by external electric fields through narrow channels.

The extensive literature on many-particle Brownian motion [1, 4, 11, 12] largely omits actively driven motion through single-file channels. Recent theoretical models [13, 14] on collective electrophoretic motion assume that the hydrodynamic coupling is set by the channel

diameter. In contrast, our work on Brownian motion demonstrated that particle coupling extends through the length of the entire channel [4]. The influence of these long-range interactions and their crucial role in transport through narrow channels is so far an unsolved question. Here, we test the key prediction of [4] that hydrodynamic interactions are crucial for the correct description of collective transport in confinement. We verify this hypothesis by combining simulations and experiments. Thereby, we report our results on density-dependent speed-up during actively-driven particle transport through narrow channels.

## Predictions

We first demonstrate the crucial role of nondecaying hydrodynamic interactions for driven particle transport by building on our finite-element simulations [4]. We will compare two examples of driving forces: electrokinetic and pressure driven. The main distinction for our problem is that electrical forces act on the individual particle, i.e. each particle can be considered to be driven by a body force. In contrast, for pressure driven transport the whole fluid in the channel moves so the particles remain stationary in the reference frame of the fluid.

For modelling electrokinetic effects we chose an axial-symmetric channel containing a spherical particle in a uniform electric field ( $E$ ), as shown in Figure 1a. The particle carries a negative surface charge, while the charge on the channel walls is varied. We assume a low Reynolds number regime and that flows have no-slip boundary conditions at the walls. The electrophoretic force drives the particle through the channel at velocity  $v_{ep}$  resulting in liquid being pushed forwards, resembling a piston effect. The resulting Poiseuille flow is indicated on the right of Figure 1a. In the case where the channel walls carry a negative charge, the well-known electroosmotic plug flow (EOF) develops with velocity  $w$  moving in the opposite direction to  $v_{ep}$  [15].

As we are unaware of any analytical solutions for our

---

\* correspondence: karolis@misiunas.com

† correspondence: ufk20@cam.ac.uk

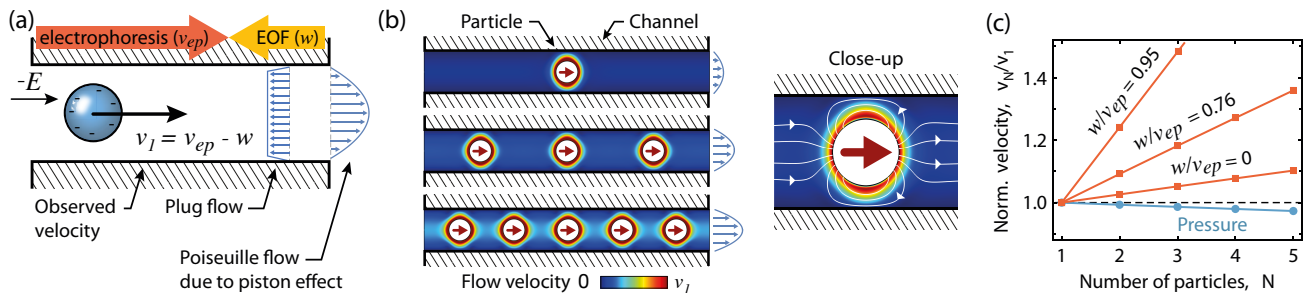


FIG. 1. Simulation of hydrodynamic flows in narrow channels containing particles driven by electric fields and pressure. (a) The applied field,  $E$ , over the channel drives a negatively charged particle through a finite channel at velocity  $v_{ep}$ , giving rise to a Poiseuille flow due to a piston effect. An electro-osmotic plug flow (EOF) caused by negatively charged walls (velocity  $w$ ) is flowing in the opposite direction. (b) Exemplary results of finite-element simulations for one, three, and five particles driven through a channel by an electric field (red arrow indicates the direction of force). The Poiseuille flow increases with particle number in the channel  $N$ . The inset shows flow close-up on one particle and the corresponding flow streamlines. (c) The predicted normalised particle velocity  $v_N/v_1$  increases with the particle number  $N$  for actively-driven particles by electric field  $E$  (red). In contrast, for pressure-driven particle  $v_N/v_1$  is linearly declining (blue).

problem, we quantify the flows using a numerical model implemented using COMSOL Multiphysics (v4.4). Our axial symmetrical model is accessible online [16]. In contrast to the literature [13, 14], we adapt periodic boundary conditions to account for the finite channels which allow for Poiseuille flows through the inlets [4]. Flows across the inlets into the reservoirs are critically important for hydrodynamic interactions. Figure 1b summarises the key results of our simulations with the color maps depicting fluid flows for 1, 3, and 5 particles. The first row of Figure 1b shows the flow velocity around a single moving particle due to electrophoretic body force (indicated by the red arrow in the particle). The particle's motion induces a finite Poiseuille flow as illustrated by the profile on the right. Increasing the number of particles by two in rows two and three, increases the magnitude of the Poiseuille flow. The enhanced net flow throughout the channel is easily observed by the change in color from dark to light blue. Importantly, increased Poiseuille flows increase the velocity of all particles.

Figure 1c shows our quantitative predictions of the simulations for particles driven by electrophoresis (red) and pressure driven flows (blue). In order to simplify the comparison we plot the predicted particle velocity  $v_N$  normalised to the velocity for one particle,  $v_1$ , as a function of  $N$ . The simulation parameters were selected to match our experiments with channel length  $L = 10 \mu\text{m}$ ; diameter  $2R = 840 \text{ nm}$ ; particle diameter  $2a = 500 \text{ nm}$ .

The first observation is that the change of  $v_N/v_1$  clearly depends on the type of driving force. For particles driven by electric fields  $v_N/v_1$  is increasing linearly with  $N$  (red lines). In contrast, particles carried by a pressure flow exhibit no speed-up (blue curve in Figure 1c), as expected [17]. The small velocity reduction  $v_5/v_1 < 1$  for  $N > 1$  is due to particles perturbing the optimal flow profile, thus slowing down the pressure induced flow that carries the particles [18].

Our simulations indicate that the velocity  $v_N$  is lin-

early proportional to  $N$ . For comparing different driving forces, we define an *interaction coefficient*  $\rho = \Delta v/v_1$ , where  $\Delta v = v_{N+1} - v_N$  is the averaged speed-up due to each additional particle.  $\rho$  can be extracted from the slope of the curves in Figure 1c. For electrophoresis,  $\rho$  ranges from 2.6% to 24.1% depending on  $w$ . For pressure driven flows we extract  $\rho = -0.69\%$  indicating a slow down of the particles with increasing density. To the best of our knowledge, this is the first quantitative prediction of a speed-up of particle transport due to long-range hydrodynamic interactions in narrow channels.

The final observation is that the EOF velocity ( $w$ ) is an important parameter as the enhancement  $v_N/v_1$  depends on  $w$ . Figure 1c shows simulations for three different surface charges resulting in  $w/v_{ep} = 0.0, 0.76$ , and  $0.95$ . As  $w$  is increased  $v_N/v_1$  is increasing and hence EOF can be used to tune particle speed-up. One important conclusion is that by controlling the channel surface charge and hence EOF we can tune  $\rho$ .

## Experimental Methods

We experimentally tested our predictions using a microfluidic device with precisely controlled channel geometry. Inside the chip, two reservoirs are connected by narrow channels of length  $L = 10.0 \pm 0.5 \mu\text{m}$  and rectangular cross-section  $800 \pm 50 \text{ nm} \times 800 \pm 50 \text{ nm}$ . Figure 2a shows an illustration of our setup, while Figure 2b shows micrographs of a typical channel. Briefly, we fabricate these chips via replica moulding of polydimethylsiloxane (PDMS), where the master is made using e-beam lithography and photo-lithography; more details are published elsewhere [18, 19]. A PDMS copy is air plasma bonded to a glass slide that is coated with a sub  $100 \mu\text{m}$  PDMS layer, ensuring that all channel walls are made out of the same material [20].

An assembled chip is filled with KCl solution con-

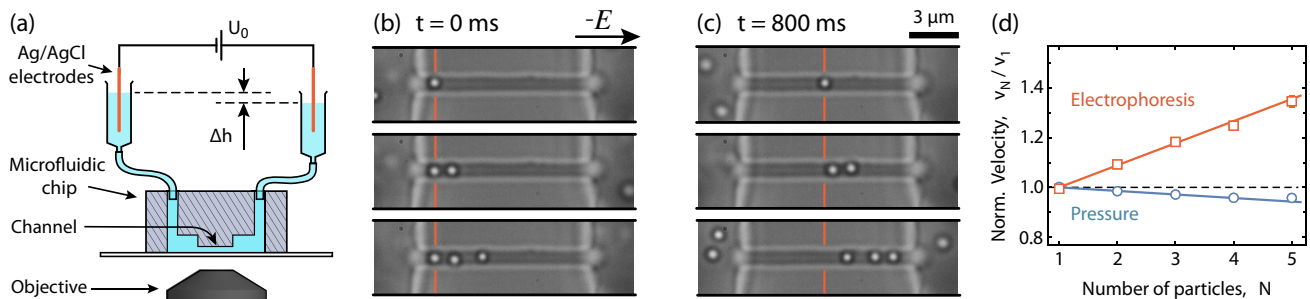


FIG. 2. Experimental comparison of particles driven through a microfluidic channel by electrophoresis and pressure flow. (a) The schematic of our setup shows two reservoirs containing the electrodes for applying electric fields. Moving the containers vertically allows for control of the pressure across the channels. (b) Micrographs show one, two, and three particles in the channel with leftmost particles aligned to the orange line. The negatively charged particles migrate in an electric field for 800 ms and the resulting micrographs are shown in (c). In (c) orange lines are aligned with the one particle case. The migration velocity increases with the number of particles in the channel. (d) The normalised particle velocity ( $v_N/v_1$ ) as a function of particle number  $N$  in the channel for electrophoretic transport (red). The data suggests linearly increase of  $v_N/v_1$  with  $N$ . Pressure driven transport (blue) is shown as control. Errors are smaller than the marker sizes.

taining spherical polystyrene particles of diameter  $2a = 505 \pm 8$  nm (Polysciences Inc; density  $\sim 5$  particle/pl). Their motion is imaged through an inverted optical microscope with a high numerical aperture oil-immersion objective ( $100\times$ ; NA 1.4; UPLSAPO) and recorded using a camera (Mikrotron MC1362) at a rate of 200 frames per second. Afterwards, the particle trajectories are extracted using our established image analysis techniques [21].

From the particle trajectories, we extract the velocity as a function of a particle number inside the channel. Only particles separated by more than  $1.2 \mu\text{m}$  are analysed, thus excluding any close range effects [4, 13]. In addition, we disregard all parts of the trajectories within  $0.5 \mu\text{m}$  of the channel ends to ensure diffusion coefficients are constant [22]. The remaining trajectory segments are averaged while retaining the particle count.

The particles are actively driven by external electric fields applied using two Ag/AgCl-electrodes submerged in the external reservoirs (see Figure 2a). They are connected to a digital to analogue converter (NI-USB-6211), which applies electric potentials up to 1 V controlled by a computer. After assembling the chip, we find the pressure equilibrium by adjusting the pressure until particles stop migrating to either side of the channel. Pressure is applied by adjusting the relative height of the external reservoirs.

### Electrophoresis

We started by measuring the velocity of 1, 2 and 3 particles in a channel under electric fields, as shown in Figure 2b. At  $t = 0$  the leftmost particles are aligned to the orange line. After 800 ms the snapshot shows the positions of the particles in Figure 2c. Evidently, the two particles travelled further than one particle in 800 ms; and three made it further than two, proving the speed-

up with the number of particles, as predicted from our simulations.

Quantitatively, Figure 2d shows  $v_N/v_1$  as a function of  $N$  for electrophoretic motion (estimated from  $\sim 38000$  video frames of more than 650 particles). The data (red) shows that  $v_N/v_1$  is linearly proportional to  $N$ , again as predicted. The measured interaction coefficient for electrophoresis is  $\rho = 9.02 \pm 0.43\%$  at 2 mM KCl and pH 7.2. Absolute velocities are reported in Table I. For comparison, the pressure driven transport through the same channel has a small negative interaction coefficient of  $\rho = -1.43 \pm 0.07\%$ , confirming the expectation from the models. Our experiment demonstrates that depending on the driving force the velocity is increasing with the number of particles in narrow channels.

Force	$v_1$ ( $\mu\text{m/s}$ )	$\Delta v$ ( $\mu\text{m/s}$ )	$\rho$ (%)
EP (Fig. 2d)	$17.48 \pm 0.08$	$1.56 \pm 0.04$	$8.9 \pm 0.2$
EP (max)	$4.49 \pm 0.05$	$1.08 \pm 0.03$	$24.1 \pm 0.6$
EP (min)	$78.9 \pm 1.2$	$1.22 \pm 0.07$	$1.54 \pm 0.08$
Pressure	$68.10 \pm 0.06$	$-0.97 \pm 0.05$	$-1.43 \pm 0.07$
Gravity	$0.23 \pm 0.02$	$0.043 \pm 0.009$	$18.9 \pm 3.4$

TABLE I. The measured velocities for a single particle in the channel ( $v_1$ ); average speed-up velocity ( $\Delta v$ ); the interaction coefficient ( $\rho$ ); and the driving potential for that particular force. EP stands for electrophoresis with the three special cases, as described in the text. Driving potential is 200 mV for electrophoresis; and 11.9 mm for pressure; and  $80^\circ$  for gravity.

$\rho$  depends on experimental parameters, such as salt concentration and pH (shown in Figures S1) through EOF. In the simplest case, consider a linear superposition of the flows induced by electrophoresis and EOF, as illustrated in Figure 1a. In experiments we observe the apparent velocity of the particle  $v_1 = v_{ep} - w$ . For multiple particles, this generalises as  $v_N \approx v_{ep,N} - w$ , where  $v_{ep,N}$  indicates the electrophoretic velocity for  $N$  particles without the EOF and the approximation comes from non-linear components that are small for our salt

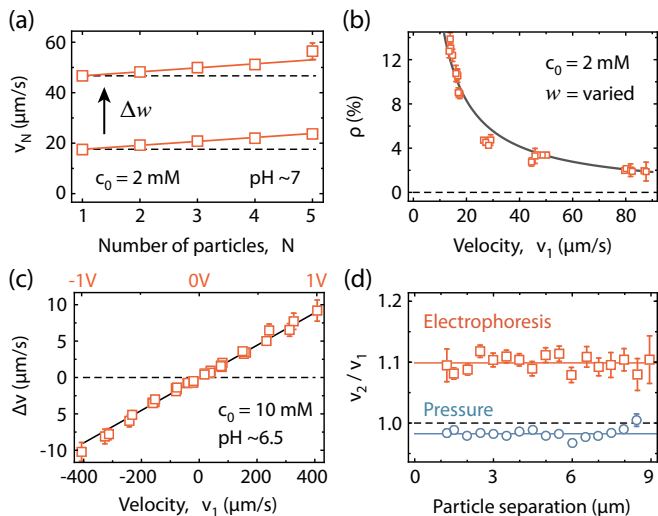


FIG. 3. (a) The velocity of  $N$  particles is increasing linearly for different wall charges indicated by a change in  $w$ . (b) Interaction coefficient  $\rho$  is shown as a function of particle velocity  $v_1$ . The black line is a weighted fit to  $\rho = \Delta v/v_1$ , where  $\Delta v = 1.59 \mu\text{s}^{-1} = \text{const.}$ . An increase of wall charge leads to higher  $w$  and hence lower  $v_1$ . (c) Speed-up velocity  $\Delta v$  as a function of  $v_1$ .  $\Delta v$  is linear in  $v_1$  and applied voltage (top axis), as expected. (d) The relative velocity of two particles  $v_2/v_1$  is independent of the inter-particle distance due to non-decaying hydrodynamic interactions.

concentrations [23]. If EOF is present,  $\rho$  depends on outside parameters controlling  $w$  while the speed-up velocity stays constant  $\Delta v \approx \text{const.}$

To test this hypothesis, we adjust the EOF by changing the surface charge density on the channel walls. In Figure 3a we changed the pH from 7.5 to 5, which decreases the surface charge density on the PDMS [15].  $v_1$  increases from  $17.5 \pm 0.1 \mu\text{s}^{-1}$  to  $46.7 \pm 0.1 \mu\text{s}^{-1}$ , but the speed-up velocity stays roughly the same at  $\Delta v = 1.56 \pm 0.07 \mu\text{s}^{-1}$  and  $\Delta v = 1.58 \pm 0.06 \mu\text{s}^{-1}$ . As a result, the interaction coefficient decreases from  $\rho = 8.8 \pm 0.3\%$  to  $\rho = 3.4 \pm 0.2\%$ , showing that the interaction coefficient can be controlled by adjusting the EOF velocity. From the relationship  $\rho \approx \Delta v/(v_{ep} - w)$ , we can maximise the interaction coefficient with electrophoretic velocity matched by the EOF velocity. Meanwhile, we can minimize the interaction coefficient when  $w = 0$ .

Experimentally we demonstrate this role of EOF by varying the surface charge of the channels by pH [15] or exposing channels to water for 12 hours and 24 hours, which reduces the surface charge on the PDMS after plasma bonding [24]. Both treatments change the EOF, while keeping the electrophoretic force constant (Figure S2). Figure 3b shows that experimental values of  $\rho$  fall on a hyperbolic curve, as expected by our simple model.

In practice, the EOF also depends on the salt concentration [15] and surfactants [25]. However, these param-

eters also affect electrophoresis, thus making the attribution of effects difficult. We explored experimental parameters and present our findings in the supplementary material [18], while highlighting two extreme cases. The highest observed interaction coefficient is  $\rho = 24.1 \pm 1.7\%$  at 4 mM KCl, pH 6, and 0.5 mM MES buffer. In contrast, the smallest observed coefficient is  $\rho = 1.54 \pm 0.08\%$  at 2 mM KCl, pH 7, and pre-filling the chip for 48 hours before the experiment. This value is close to our simulation prediction of 2.6% with  $w/v_{ep} = 0$ , suggesting that our simulations accurately capture the physics.

Although the interaction coefficient varies with the EOF velocity, it stays constant for different driving potentials, as shown in Figure 3c. The speed-up velocity linearly increases with  $v_1$  and the applied electric potential, where  $\rho$  stays constant at 2.3%. These results affirm our choice of measuring the interactions using the interaction coefficient.

Finally, we further test the hydrodynamic interaction hypothesis by measuring two particle velocity as a function of their separation distance, as shown in Figure 3d. It suggests the velocity is independent of a particle-particle distance. We see the same characteristic in our hydrodynamics simulations (Figure S3) and it was observed between Brownian particles in channels [4], suggesting that the particle speed-up is caused by the characteristic nondecaying hydrodynamics interactions.

## Gravity

Finally, we must demonstrate that these hydrodynamic interactions are universal for other actively driven particles in channels, as predicted by our models. To achieve this, we use a different body force – gravity.

Gravity experiments are performed in the same microfluidic channels, but with gold particles of diameter  $2a = 400 \pm 50 \text{ nm}$  (supplied by CytoDiagnostics Inc; 0.1 mM PBS; 1 mM KCl). Gold particles have much higher mass density than water and thus they sink. An assembled chip is mounted on a custom built rotatable microscope, as shown in Figure 4 inset. In contrast with the experiments using the pressure or the electric fields, gravity pulls the particles directly downwards without focusing them into the channels. This reduces the number of particles entering the channels and thus increases the uncertainty in our measurements ( $\sim 313000$  frames recorded at 30 fps of more than 330 particles). In addition, the  $\Delta v$  measurements have high variance due to very slow particle migration that is comparable in magnitude with Brownian motion (see Table I).

Figure 4 shows that gravity exhibits the speed-up effect, as expected from a body force. A weighted fit gives an interaction coefficient of  $\rho = 18.9 \pm 3.4\%$ , which agrees well with the corresponding simulation value of 17.8% ( $2a = 400 \text{ nm}$ ; no electrokinetic effects). Our experiment confirms that the nondecaying hydrodynamic



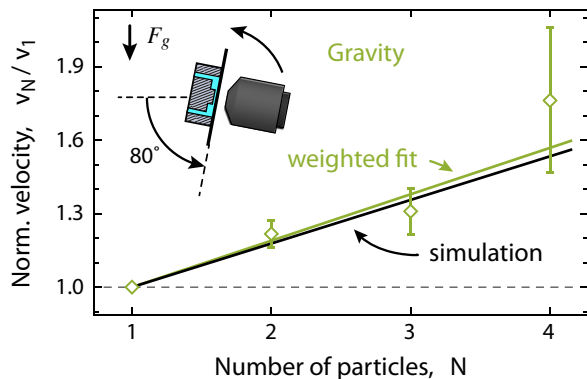


FIG. 4. Normalised particle velocity as a function of the particle number inside a channel for gravity (green) propelled particles compared to simulation results (black). Gravity experiments have the highest relative speed-up, suggesting that it produces the strongest particle-particle interactions. Inset illustrates the setup for gravity experiments.

interactions persist for gravity propelled particles, thus suggesting that the speed-up effect is universal for actively driven particles.

### Discussion

Our simulations are in agreement with our experiments, reproducing the linear speed-up with particle number, distance-independent interactions, and the approximate magnitudes for interaction coefficients. Quantitatively, the prediction values are also close, especially considering that we only have a single fitting parameter for electrophoresis – the EOF velocity,  $w$ . The differences can be explained by the approximations in our simulations: particles move on the centreline of the channel without rolling. For electrophoresis simulations, we used Debye-Hckel approximation for the ion distributions. For gravity simulations, we excluded all electro-kinetic effects and did not account for variability of particle sizes. These points should be addressed with more sophisticated simulations [22]. Nonetheless, we think our model captures the important physics and agrees well with our experiments.

The collective speed-up can easily be controlled, allowing for new technological applications. For example, we built a novel device using these interactions – a density selective channel. It permits transport through the channel, only if the particle density is high enough. The supplementary information includes a video demonstration [18]. The device has electrophoresis driving particles to the right, while a pressure flow drives them in the opposite direction. The driving potentials are carefully chosen to be exactly the same, thus preventing single particles from moving across the channel. However, when two or more particles enter the channel, the speed-up effect allows them to migrate through the channel.

Thus, transport can only happen at higher particle densities. Such density filter could be used as a sensor or as a catalyst for dimer or polymer production.

The reported interactions also have important implications for understanding natural phenomena. We predict faster transport through channels at higher particle density. The speed-up is not limited to tightly confined particles and should persist for larger channels ( $a/R < 0.3$ ). In a large channel, each particle’s piston-like contribution is small but the collective action of many particles should result in a net speed-up [18]. As a consequence, we predict that particle transport rate through channels is a super-linear function of particle density. These interactions may explain some of the peak tailing observed in electrochromatography or chromatography centrifuges because collectively particles travel faster than the isolated particles [26]. In addition, biological environments are good examples of high-density systems, where such interactions could affect the transport rates through membrane protein channels.

Further investigations are necessary to fully understand this phenomenon and its implications. In particular, we predict that self-propelled particles in confinement will be strongly affected by this phenomenon. In addition, our simulations suggest that particle surface properties also affect the interaction strength (see supplementary material [18]), thereby this phenomenon may allow for probing of the electrical double layer.

In conclusion, we have shown that particle transport velocity through channels increases with the particle number. We experimentally demonstrated that this happens with electrophoretically and gravity propelled particles but does not happen for pressure propelled particles. In addition, the interaction strength can be controlled by adjusting the electro-osmotic flow in the channels. Our models suggest that the interactions are carried by hydrodynamics, where a piston-like motion of particles induces a flow throughout the entire channel. These findings have far-reaching implications for transport through protein channels and enable novel technological applications.

### Acknowledgements

We are grateful to Soichiro Tottori, Stefano Pagliara, Eric Lauga, Nicholas A.W. Bell, Vahe Tshitoyan, and Alexander Ohmann for useful discussions. K.M. and U.F.K. acknowledge funding from an ERC consolidator grant (Designerpores 647144).

- 
- [1] Wei, Q.-H., Bechinger, C. & Leiderer, P. Single-file diffusion of colloids in one-dimensional channels. *Science* **287**, 625–627 (2000).
  - [2] Secchi, E. *et al.* Massive radius-dependent flow slippage in carbon nanotubes. *Nature* **537**, 210–213 (2016).

- [3] Radha, B. *et al.* Molecular transport through capillaries made with atomic-scale precision. *Nature* **538**, 222–225 (2016).
- [4] Misiunas, K., Pagliara, S., Lauga, E., Lister, J. R. & Keyser, U. F. Nondecaying hydrodynamic interactions along narrow channels. *Physical Review Letters* **115**, 038301 (2015).
- [5] Truskey, G. A., Yuan, F. & Katz, D. F. *Transport phenomena in biological systems* (Pearson Prentice Hall, 2009).
- [6] Sliwoski, G., Kothiwale, S., Meiler, J. & Lowe, E. W. Computational methods in drug discovery. *Pharmacological Reviews* **66**, 334–395 (2013).
- [7] Clarke, J. *et al.* Continuous base identification for single-molecule nanopore DNA sequencing. *Nature Nanotechnology* **4**, 265–270 (2009).
- [8] Bell, N. A. W. & Keyser, U. F. Digitally encoded DNA nanostructures for multiplexed, single-molecule protein sensing with nanopores. *Nature Nanotechnology* **11**, 645–651 (2016).
- [9] Ingham, D. B. & Pop, I. *Transport phenomena in porous media* (Elsevier Science, 1998).
- [10] Pikul, J. H., Gang Zhang, H., Cho, J., Braun, P. V. & King, W. P. High-power lithium ion microbatteries from interdigitated three-dimensional bicontinuous nanoporous electrodes. *Nature Communications* **4**, 1732 (2013).
- [11] Diamant, H. Hydrodynamic interaction in confined geometries. *Journal of the Physical Society of Japan* **78**, 041002 (2009).
- [12] Cui, B., Diamant, H. & Lin, B. Screened hydrodynamic interaction in a narrow channel. *Physical Review Letters* **89**, 188302 (2002).
- [13] Hsu, J. P., Ku, M.-h. & Kao, C.-y. Electrophoresis of two identical cylindrical particles along the axis of a cylindrical pore. *Industrial & Engineering Chemistry Research* **44**, 1105–1111 (2005).
- [14] Hsu, J. P. & Yeh, L. H. Electrophoresis of two identical rigid spheres in a charged cylindrical pore. *Journal of Physical Chemistry B* **111**, 2579–2586 (2007).
- [15] Kirby, B. J. & Hasselbrink, E. F. Zeta potential of microfluidic substrates: 2. Data for polymers. *Electrophoresis* **25**, 203–13 (2004).
- [16] Misiunas, K. COMSOL simulation code (2017). URL [github.com/kmisiunas/speed-up-simulation](https://github.com/kmisiunas/speed-up-simulation).
- [17] Happel, J. & Brenner, H. *Low Reynolds number hydrodynamics* (Springer, 1981).
- [18] Supplementary Material found along with this article (2018).
- [19] Pagliara, S., Chimereel, C., Langford, R., Aarts, D. G. a. L. & Keyser, U. F. Parallel sub-micrometre channels with different dimensions for laser scattering detection. *Lab on a Chip* **11**, 3365 (2011).
- [20] Deshpande, S., Caspi, Y., Meijering, A. E. C. & Dekker, C. Octanol-assisted liposome assembly on chip. *Nature Communications* **7**, 10447 (2016).
- [21] Dettmer, S. L., Keyser, U. F. & Pagliara, S. Local characterization of hindered Brownian motion by using digital video microscopy and 3D particle tracking. *Review of Scientific Instruments* **85**, 023708 (2014).
- [22] Dettmer, S. L., Pagliara, S., Misiunas, K. & Keyser, U. F. Anisotropic diffusion of spherical particles in closely confining microchannels. *Physical Review E* **89**, 062305 (2014).
- [23] Liu, Y.-w., Pennathur, S. & Meinhart, C. D. Electrophoretic mobility of a spherical nanoparticle in a nanochannel. *Physics of Fluids* **26**, 112002 (2014).
- [24] Bodas, D. & Khan-Malek, C. Hydrophilization and hydrophobic recovery of PDMS by oxygen plasma and chemical treatment An SEM investigation. *Sensors and Actuators B: Chemical* **123**, 368–373 (2007).
- [25] Makamba, H., Kim, J. H., Lim, K., Park, N. & Hahn, J. H. Surface modification of poly(dimethylsiloxane) microchannels. *Electrophoresis* **24**, 3607–3619 (2003).
- [26] Sun, Y., Kwok, Y. C. & Nguyen, N. T. Modeling and experimental characterization of peak tailing in DNA gel electrophoresis. *Microfluidics and Nanofluidics* **3**, 323–332 (2007).